Millimeter Wave Indoor SAR Sensing Assisted With Chipless Tags-Based Self-Localization System: Experimental Evaluation

Aman Batra, *Member, IEEE*, Ali Alhaj Abbas, Jesús Sánchez-Pastor, *Graduate Student Member, IEEE*, Mohammed El-Absi, *Member, IEEE*, Alejandro Jiménez-Sáez, *Member, IEEE*, Maher Khaliel, Jan Barowski, *Senior Member, IEEE*, Michael Wiemeler, Diana Göhringer, *Member, IEEE*, Ilona Rolfes, *Senior Member, IEEE*, Rolf Jakoby, *Member, IEEE*, and Thomas Kaiser, *Senior Member, IEEE*

***Abstract*—This article addresses indoor environment mapping by employing the synthetic aperture radar (SAR) technique at millimeter wave (mmWave) frequencies. The mmWave-based SAR can provide a high-resolution map, for example, of an emergency scenario like a burning room. The high-resolution map drives a new era of SAR applications such as object detection, classification, characterization, and precise localization. A major requirement at high frequencies is the precise knowledge of SAR trajectory, where radar sensors are mounted on a mobile platform such as a drone or unmanned aerial vehicle (UAV). State-of-the-art localization methods such as global positioning system (GPS)-aided inertial measurement units (IMUs) are not valid due to limited coverage and accuracy. One of the primary solutions could be the SAR assisted with an indoor localization system, which is exploited in the work. The presented indoor localization system comprises two types of passive chipless frequency-coded tags, based on dielectric resonators (DRs) and frequency-selective surfaces. In this work, first, the proposed method of integrating SAR and localization systems is evaluated in a single-tag environment. Further, a version of a room equipped with a multitag system is considered for real-time applications, and a successful demonstration of indoor environment mapping for the frequency spectrum of 75–110 GHz is presented.**

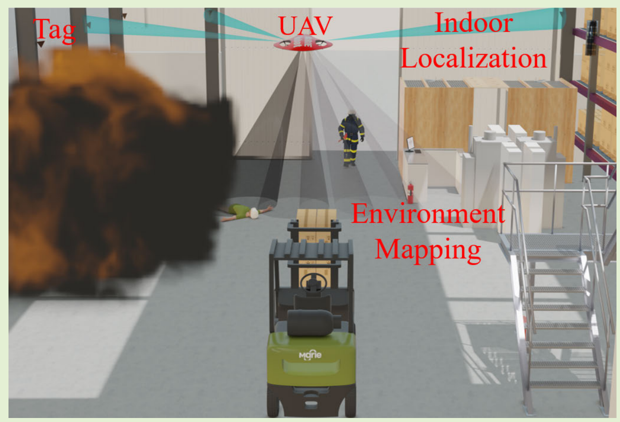

***Index Terms*—High-resolution synthetic aperture radar (SAR), indoor imaging, mmWave identification, mmWave indoor mapping, passive tag localization, radar imaging.**

Manuscript received 14 October 2023; accepted 5 November 2023. Date of publication 20 November 2023; date of current version 2 January 2024. This work was supported in part by the Deutsche Forschungsgemeinschaft through TRR 196 MARIE Projects S04, S05, M04 and C09, under Grant Project-ID 287022738; and in part by the Open Access Publication Fund of the University of Duisburg-Essen. The associate editor coordinating the review of this article and approving it for publication was Prof. Huang Chen Lee. *(Corresponding author: Aman Batra.)*

Aman Batra, Ali Alhaj Abbas, Mohammed El-Absi, Maher Khaliel, Michael Wiemeler, and Thomas Kaiser are with the Institute of Digital Signal Processing, University of Duisburg-Essen, 47057 Duisburg, Germany (e-mail: aman.batra@uni-due.de; ali.alhaj-abbas@uni-due.de; mohammed.el-absi@uni-due.de; maher.ahmed@uni-due.de; michael.wiemeler@uni-due.de; thomas.kaiser@uni-due.de).

Jesús Sánchez-Pastor, Alejandro Jiménez-Sáez, and Rolf Jakoby are with the Institute of Microwave Engineering and Photonics, Technische Universität Darmstadt, 64283 Darmstadt, Germany (e-mail: jesus.sanchez@tu-darmstadt.de; alejandro.jimenez_saez@tu-darmstadt.de; rolf.jakoby@tu-darmstadt.de).

Jan Barowski and Ilona Rolfes are with the Institute of Microwave Systems, Ruhr University Bochum, 44801 Bochum, Germany (e-mail: jan.barowski@rub.de; ilona.rolfes@rub.de).

Diana Göhringer is with the Chair of Adaptive Dynamic Systems, Technische Universitaet Dresden, 01069 Dresden, Germany (e-mail: diana.goehringer@tu-dresden.de).

Digital Object Identifier 10.1109/JSEN.2023.3332431

I. Introduction

THE millimeter wave (mmWave) spectrum, defined for the frequencies ranging from 30 to 300 GHz, is actively explored in the sector of radar sensing due to the available large bandwidth and short wavelengths. The most commonly used microwave spectrum below 30 GHz provides large sensing or propagation range but limited spatial resolution. The spatial resolution (range and angular) is directly proportional to bandwidth, carrier frequency, and antenna length [1], [2]. Hence, the mmWave spectrum seems promising in this context, as it offers high resolution in comparison to the microwave spectrum and also possesses better penetration capabilities than the optical spectrum. The mmWave spectrum extends the radar applications in various sectors like automotive, security, non-destructive testing, and material characterization due to unique signatures of some materials at this frequency region. One of the emerging applications is radar-based indoor environment mapping, which can be considered as an adaptation of a similar approach, popularly known as simultaneous localization and mapping (SLAM), from the well-established optical spectrum. SLAM aims in constructing an unknown environment map along with localization of the static or dynamic objects. It has a variety of applications in the sector of robotics and automotive such as autonomous navigation of drones and automobiles [3], [4]. SLAM in the optical spectrum is broadly classified into vision-based and light detection and ranging (LiDAR)-based SLAM.

On the one hand, vision-based SLAM processes visual inputs from optical sensors such as stereo, monocular, and RGB-D cameras. On the other hand, LiDAR-based SLAM is an active system where laser sources and detectors are employed. Here, the imaging scene is reconstructed by processing the time-of-flight (ToF) information provided by the LiDAR sensor [5], [6]. In some cases, both methods can be combined, as demonstrated in [3] and [4]. Both approaches have certain strengths and weaknesses. For example, vision-based SLAM is highly sensitive to lightning conditions, whereas LiDAR is limited with weather conditions such as rain and fog [3]. As aforementioned, these approaches operate at optical frequencies, which offer very high spatial resolution due to the large available bandwidth and short wavelengths. However, the optical spectrum is considered non-penetrating. Hence, it cannot provide look-through sensing, where the radar technology is the only possible solution.

An example application scenario could be an indoor hazardous environment and rescue mission, where the objective is to obtain an environment map. In this case, the optical sensors might not offer useful information when a target of interest is obscured by smoke, fire, or hidden by other opaque objects. For example, environment mapping using optical sensors is shown in [7] and [8]. The resulting images are of very high-resolution, but non-penetrating as nothing is mapped behind the doors and walls in [7]. Similarly, in the case of considered indoor objects in [8], only the object's front surface is mapped. In contrast, microwave sensors offer higher penetration depth, but with a limited resolution. This is demonstrated in [9] and [10], where indoor environment mapping is shown microwave sensors around the center frequency of 1.35 and 5.8 GHz, respectively. Conversely, mmWave sensors can provide a high-resolution room map. The achieved map can be further analyzed for material characterization, object localization, detection, and classification. Detecting and localizing unconscious human beings covered by smoke or estimating the danger from high-voltage electrical cables are common examples.

In the focus of the aforementioned example, this article addresses radar-based indoor environment mapping at mmWave spectrum. Here, the mapping consists of identification of passive chipless tags, localization of mmWave sensors and objects, and imaging of environment. This objective of identification, localization, and imaging is achieved by employing synthetic aperture radar (SAR) technique [11] assisted with localizable chipless tags [12], [13]. In [12], simulation analysis is in the foreground for the integration of the proposed method along with the impact of the small motion errors on SAR image. The technique of localization with chipless tags is investigated with measurements in [13] at microwave spectrum and simulation analysis concerning the effective area of the reader's antenna is performed at sub-mmWave band. The article focuses on the evaluation and demonstration of the proposed indoor mapping by using SAR assisted with the localization system at mmWave band.

SAR is a remote sensing technique mainly used for 2-D and 3-D imaging. In this technique, a large aperture is synthesized to provide high angular resolution. The radar sensors are mounted on a mobile platform, which follows a certain trajectory to form a synthetic aperture and radiate electromagnetic (EM) waves toward the target. Backscattered signals are recorded and processed for image reconstruction [11], [14]. SAR technique implementation requires very high positioning accuracy of the radar sensors [12]. In an outdoor environment, a global positioning system (GPS) along with an inertial measurement unit (IMU) is used to obtain the localization information of the sensors. This approach cannot be applied for mmWave SAR sensing in an indoor environment. First, the GPS does not provide coverage in the indoor environment. Second, neither the GPS nor the state-of-the-art compact IMU provides the required localization accuracy at mmWave frequencies. One possible solution is to implement an indoor localization system. In [15], [16], [17], and [18], mmWave SLAM is discussed without a priori knowledge of the surrounding environment and is based on the detection of environmental echoes. Most of them achieve localization with sub-cm accuracy in simulated setups, with [16] presenting a sub-cm resolution in real-world measurements. Moreover, an overview of different state-of-the-art localization approaches at mmWave frequencies is available in [19]. The performance metric in [19] presents that the localization accuracy primarily is in the range of sub-m to sub-10 cm. Whereas mmWave SAR required a positioning accuracy in the order of sub-mm, a detailed analysis of positioning accuracy concerning frequency and radar orientation is available in [12].

This article explores a novel solution of SAR aided by self-localization in mmWave frequencies by employing cooperative and chipless radar landmarks or tags. Cooperative because they present frequency coding, allowing to distinguish between them and to establish them as reference positions for localization, and chipless because they do not employ power sources, which allows easy integration within an existing infrastructure. In this article, frequency-coded corner reflectors (CRs) are used as landmarks for localization and identification. The coded reflectors are the result of joining a coding structure with a triangular trihedral CR. The coding structure provides identification and the reflector allows a high radar cross section (RCS) response over a wide angle. Combining coding structures with high RCS reflectors has been introduced in the literature to mainly enhance the RCS and retrodirectivity. In [20], [21], and [22], frequency-coded lenses are proposed based on combining several resonant structures with homogenous and Luneburg lenses. However, homogenous lenses show a limited increase in RCS with the enlargement of the lens size because of high structural reflections, while Luneburg lenses are difficult to fabricate at mmWave and sub-mmWave spectrum. Instead, a coding filter has been attached to the surface of dihedral reflectors [23] or in front of trihedral reflectors [24], [25]. These approaches can boost the RCS to any level by increasing the reflector dimension. In this article, two models are applied based on placing a dielectric resonator (DR) array and frequency selective surface (FSS) in front of a trihedral CR [25].

In terms of the article's contributions, it validates a novel SAR solution aided by an indoor passive localization system through experimental results. Further, to realize the potential of mmWave SAR in indoor environments as described, the proposed solution holds a substantial advantage in achieving the necessary sub-millimeter localization accuracy and acquiring high-resolution images. A comprehensive overview of the method, including the associated signal processing models for SAR and the localization system, is provided in Section II. The presented workflow encompasses tag identification, mobile platform localization, object imaging, and object localization. In Section III, we describe FSS- and DR-based landmarks and provide a comparative summary of the two approaches. Further, Section IV provides detailed descriptions of the single-tag measurement setups used for evaluating the integration of SAR and localization systems. Additionally, with a focus on coverage enhancement, Section V explores a more intricate multitag setup that closely mirrors a practical environment. Lastly, in Section VI, a conclusion is provided along with future prospects.

II. Theoretical Modeling

This section addresses the theoretical model associated with indoor mapping. The proposed method is acquired by the integration of SAR and indoor localization techniques. Therefore, first, this section presents the signal processing associated with both the techniques and then explains the approach of localization-assisted indoor SAR sensing.

A. Imaging

In the radar domain, SAR is a well-established imaging technique. It is developed in the 1950s as an alternative to the optical imaging system. Presently, it is used in a wide variety of applications such as surveillance/security, meteorology, concealed and hidden object sensing [11], [14]. The general principle for SAR in the indoor environment is illustrated in Fig. 1, where the objective is to create a 2-D image of the environment. In the presented imaging scene, the mmWave sensors are mounted on a mobile platform, which could be an unmanned aerial vehicle (UAV) or unmanned ground vehicle (UGV). The EM waves are transmitted toward the targets along the range direction. A SAR aperture is formed with movement of UAV/UGV along the azimuth direction. For the presented imaging geometry in Fig. 1, the range and azimuth directions are along the x- and y-axis, respectively. To form a 2-D image of the ground targets in the x–y plane, the backscattered waves are received and recorded by the sensors providing the raw data.

1) Raw Data Acquisition and Image Reconstruction: The raw data formation can be modeled by considering a transmit signal $p(t)$ which could be a chirp, Gaussian, or single/multitone. For transceiver at aperture position u, where $u \in (u_1, u_N)$ and N is the total number of aperture positions, the received signal from K scatterers can be given by

$$s(t, u) = \sum_{k=1}^{K} \sigma_k p(t - t_k) \tag{1}$$

where σ_k is the reflectivity from kth scatterer, $t_k = (2R_k/c)$ is round trip delay time, c is the speed of light, and R_k is

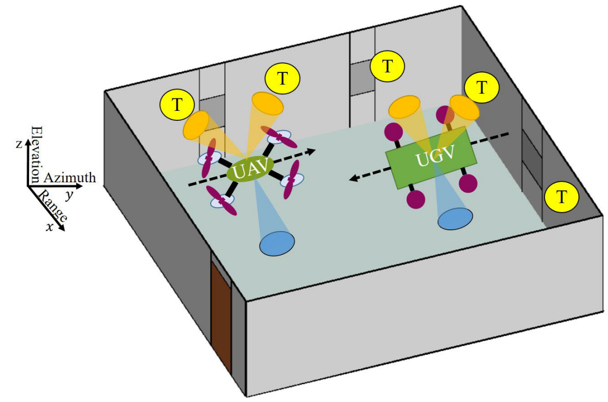

Fig. 1. UAV- or UGV-based indoor SAR mapping scene assisted with passive-tags-based localization system.

the slant range between the transceiver and kth scatterer. The received signal is accumulated at all aperture positions and a 2-D raw data for image reconstruction is formed.

For image reconstruction, the raw data is processed with time- or frequency-domain image reconstruction algorithm. For example, *backprojection alogrithm* (BPA) is a time-domain algorithm and *Omega-K* and *Range Doppler Algorithm* (RDA) are frequency-domain algorithms [11], [14]. In this article, BPA is used due to its simplicity and accuracy. Besides, the BPA is more robust toward motion errors in comparison to frequency-domain algorithms but requires high computational power [26]. However, the algorithm lacks in data dependencies and inherits parallelism to address real-time imaging.

In this article, for the vector network analyzer (VNA)-based testbed, the captured raw data in frequency domain defined by S_f is first upsampled for smoother transition to time-domain s_t. The upsampling also provides compatibility with the 2-D imaging grid $\mathbf{I}$. Based on BPA, the pixel value at location (x_i, y_i) is calculated by

$$I(x_i, y_j) = \sum_{n=0}^{N} s_t(t_{ij}, u_n) \exp(-\text{j}4\pi f_{\min} R_{ij}(u_n)/c) \tag{2}$$

where t_{ij} is round trip delay for the scatterer at the pixel position (x_i, y_j) in $\mathbf{I}$, $f_{\min}$ is the minimum frequency of upsampled raw data, and $R_{ij}(u)$ is the slant range for the aperture position u. Moreover, a comprehensive description of image reconstruction with BPA is available in [1] and [14].

2) Spatial Resolution: For the presented case of 2-D imaging, the spatial resolution is classified into range and azimuth resolution. The resolution defines the minimum resolvable distance between two scatterers. The range resolution is given by

$$r_x = \frac{c}{2B_w} \tag{3}$$

where B_w is the system bandwidth. At mmWave frequencies, higher bandwidth is available which results in providing better resolution. For the considered bandwidth of 35 GHz in the spectrum range of 75–110 GHz, the range resolution is ∼4.3 mm.

The cross-range or azimuth resolution r_y is determined by the antenna half-power beamwidth and given as $r_y \approx \lambda R_{\text{ref}}/2L_s$, where R_{ref} is the reference range between the sensor and target scene center, λ is the signal wavelength, and L_s is the synthetic aperture length. In consideration of $L_s = \lambda R_{\text{ref}}/L_a$, where L_a is the antenna length, r_y can be derived as

$$r_y = L_a/2. \tag{4}$$

It is independent of the propagation range [1], [2] and defined as the maximum achievable azimuth resolution in far-field region. At mmWave spectrum, compact antennas are available and hence provide high azimuth resolution if the condition of required L_s is full-filled.

B. Localization

Sub-mm localization is essential for the mmWave SAR process [12], where a chipless radio frequency identification (RFID)-based localization system proposed [13] is considered in this work. In this system, the UAV acts as a reader, which collects measurements from the reference chipless tags in order to perform self-localization. For 2-D localization, a minimum of three reference chipless tags is required, where the localization is performed through two phases: The first phase is ranging; and the second is lateration phase. For ranging, the time-domain signal is utilized after post-processing using matched filter in order to estimate return ToF (RToF) or round trip delay time, which is used to find the distance between the reader and the tags [13], [27]. Following the ranging phase, lateration leverages these distance measurements to ascertain the reader's position. In this phase, the trilateration algorithm is deployed to ascertain the reader's location, relying on geometric principles that hinge on the Euclidean distance between the target and a minimum of three anchors. Algorithms as linear least square (LLS) can be used to estimate the position of the reader from the estimated distances from ranging step. A further detailed description of the signal processing associated with the proposed localization system is available in [13] and [27].

C. Indoor Mapping

The indoor SAR mapping scene assisted with the passive chipless tags is shown in Fig. 1, where the mmWave radar sensors mounted on a UAV/UGV simultaneously radiate along ground targets and tags, and record the backscattered signals. The tags are represented with the yellow circles in Fig. 1.

For full-room coverage, multiple tags are mounted on the walls and ceiling. An optimized placement of the tags for maximum coverage is available in [28]. During the placement of the tags at any time frame, it is assumed that the tags precise positions in 3-D-space with respect to the room geometry are acquired and stored in the database. The information will be used for the localization of UAV/UGV. Although, the tags position is predefined but the environment is still unknown to the radar system as the position of UAV/UGV in 3-D-space is unavailable. Therefore, as an initial stage, a 360° scanning is implemented to estimate the UAV/UGV reference position. Moreover, the simultaneous excitation toward the target/objects (shown with blue beam footprint in Fig. 1) and tags (shown with orange beam footprint in Fig. 1) can be achieved using beamforming techniques with multiple-input–multiple-output (MIMO) systems. The vision of the proposed indoor mapping scheme is to acquire.

1) Identification of tags.
2) Localization of UAV.
3) Image of objects or environment.
4) Localization of objects.

For SAR sensing, precise estimation of the UAV trajectory is provided by the proposed sub-mm passive chipless tags-based localization system. Based on the trajectory estimation, the SAR image of the ground objects or indoor environment is reconstructed. SAR sensing also provides the localization of the objects in reference to the implemented trajectory. The provided objects localization can be mapped to the actual position of the objects, if the trajectory information is available in reference to room geometry and dimensions. For the presented case of indoor mapping, as described, the proposed localization system provides the trajectory information. Hence, indoor objects can be localized.

The vision is investigated with an experimental setup. The objective is to validate the vision of mmWave sensor localization, and imaging and localization of in-room objects. For localization, only the azimuth positions are primarily in focus. In case of 2-D imaging, the SAR trajectory is implemented along the azimuth direction. Hence, the range and elevation directions are constant. Currently, the focus is only on the integration and evaluation of the SAR and localization system. Although, in a realistic scenario, there will be deviations along all the axis as the UAV is highly unstable. At high frequencies, the impact of small deviations is large due to the trajectory deviation being in the range of carrier wavelength. In terms of positioning accuracy requirement with SAR, the theoretical limit based on Fraunhofer far-field condition is $\lambda/16$ [29], [30]. However, there can be different positioning accuracy requirements along the different axis as presented in [12] and [31]. As an example, for the presented case in [12], the accuracy up to 3λ and 5λ is acceptable with some artifacts. The non-ideal trajectory or trajectory deviation is not of focus in this article. Here, the primary objective is the demonstration of the indoor mapping with SAR technique at mmWave spectrum assisted with the localization system.

III. Indoor Landmarks Design

For localization and identification, unsynchronized passive landmarks are employed based on frequency-coded CR. Identification is achieved in frequency domain by placing a coding particle in front of the CR as shown in Fig. 2. Two different coding structures are considered to create different tags, namely FSS and DR. Both tags are based on the same principle to encode it in the frequency domain. Considering a mono-static radar system, tags are identified by a notch in the backscattering, which corresponds to the resonance frequency of the coding structure.

The frequency response of the combination is a large RCS over a wide range of frequencies, thanks to the CR, with a deep notch referred to the resonance frequency. This would be transferred into the time domain to an early narrow pulse caused by the CR followed by a ringing tail caused by resonance. Therefore, a high-ranging accuracy can be reached which is dependent on the large sweep bandwidth of the interrogator, not by the narrow resonant bandwidth of the coding structure. Moreover, any required RCS can be obtained by scaling up

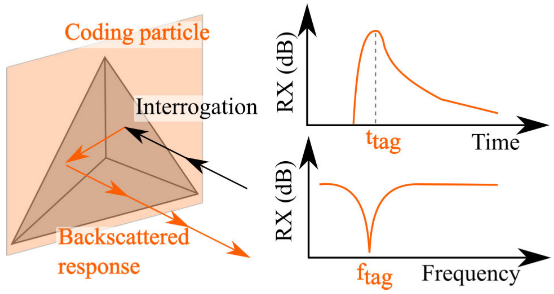

Fig. 2. Retroreflective landmark's operating principle.

TABLE I
DESIGN PARAMETERS FOR THE TWO FSS

Design parameter	Ref. [24]	FSS 1	FSS 2
Resonance frequency	78 GHz	90 GHz	107 GHz
Dipole length	1.48 mm	1.371 mm	1.154 mm
Dipole width	0.25 mm	0.232 mm	0.195 mm
Unit cell width	2.26 mm	2.093 mm	1.763 mm
Framed	No	Yes, FR-4	Yes, FR-4

the structure dimensions without losing the spectral signature, thereby allowing for long-range localization.

This section is structured as follows. First, the design of an FSS-based passive chipless tag is presented, and its frequency results are discussed in terms of identification. Then, the DR-based passive chipless tag is introduced.

A. Frequency Selective Surface

FSS are periodic structures whose resonance frequency can be engineered to present stopband or passband characteristics, depending on the application [32]. Owing to their periodicity, their analysis can be reduced to a single unit cell of the structure.

In this work, two landmarks are implemented employing a 5 × 5 cm FSS, presenting a stopband region at 90 and 107 GHz, respectively. This corresponds to the identification frequency of the tag. The structures are based on the work by Jiménez-Sáez et al. [24], where the measurement setups employed in this section to characterize the FSS and the corresponding landmark are also described. The FSS is composed of cross-dipoles etched on a Rogers RT/duroid 5880 substrate, with a substrate thickness of 127 μm and a copper thickness of 35 μm. The parameters of the unit cell for both FSS are presented in Table I. Owing to the very thin substrate used, the FSS is extremely flexible, which makes its manipulation complicated. Thus, an FR-4 scaffolding is manually pasted to the FSS, as presented in the inset of Fig. 3. Since the frame is located on the borders of the structure and small compared to its whole size, the response remains unchanged.

The transmission coefficient S_{21} for the FSS designed to resonate at 107 GHz is presented in Fig. 3, where there is no difference in the resonance frequency between the unframed structure and the final one, but there is an improvement in the notch depth for the latter. The resonance frequency of the fabricated structure is at 105 GHz, which means a shift of 2 GHz from the simulation results, attributed to manufacturing inaccuracies.

The landmark is displayed in Fig. 4. It is conformed by placing the FSS and a trihedral CR with an edge length of 3 cm in an FDM-printed supporting structure. The FSS is inserted

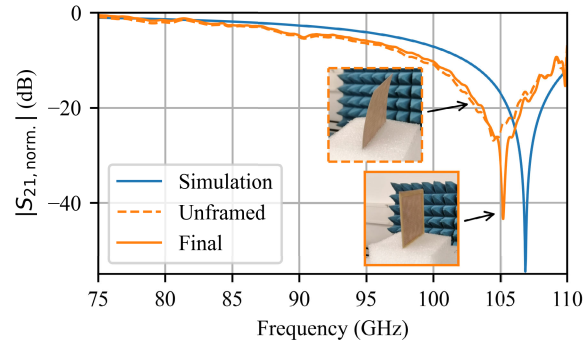

Fig. 3. Simulated and measured FSS's S_{21}. The flexible and framed structure are displayed in the insets.

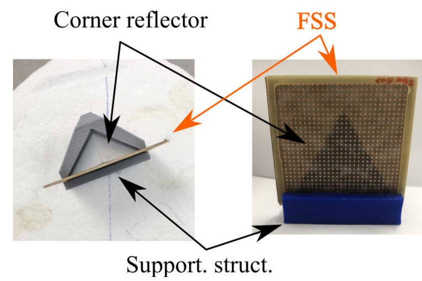

Fig. 4. FSS-based indoor tag.

in a slot, whereas the CR is located on the ramp designed for this purpose. Then, the weight of the CR sticks it to the FSS, enclosing it completely.

The tag's measured reflection coefficient, S_{11}, for several angles is presented in Fig. 5(a). It is appreciable that the responses present a notch at 105 GHz, except for the response at the frontal incidence (0°). In this case, the FSS's specular reflection is mixed with the landmark's backscattered response at the receiver. The specular reflection can be filtered out in the time domain employing time gating with window spans of approximately 100 ps, although this is not easy to accomplish in real-world operation.

The radar cross section (RCS) measures the power backscattered by a structure independently of its distance to a receiving antenna. To compute the landmark's RCS, the same CR present on it is used as reference. When the measuring setup is the same for both tag and reference CR measurements, the RCS can be calculated as

$$\sigma_{\text{landmark}} = \frac{\left|S_{11\_\text{landmark}}\right|^2}{\left|S_{11\_\text{CR}}\right|^2}\sigma_{\text{CR}} \tag{5}$$

where S_{11_landmark} and S_{11_CR} are the measured scattering parameters of the landmark and CR and σ_{CR} is the analytical RCS of the CR in bore-sight, in this case -5.96 dBm^2 for a CR with an edge length of 3 cm.

The monostatic RCS between ±40° for the FSS-based tag is shown in Fig. 5(b). On it, where less received power is represented by darker colors and vice versa, higher backscattered power is depicted by bright colors. It is noticeable that the notch at 105 GHz between −40° and −6° and from 6° to 40°. Furthermore, between ±30° and ±40°, there are multiple high-magnitude ripples, which are attributed to an interaction between the FSS and the CR. The FSS is not acting as a perfectly transparent wall for the spectrum that lies outside-of-resonance, but it is reflecting some of the frequencies from

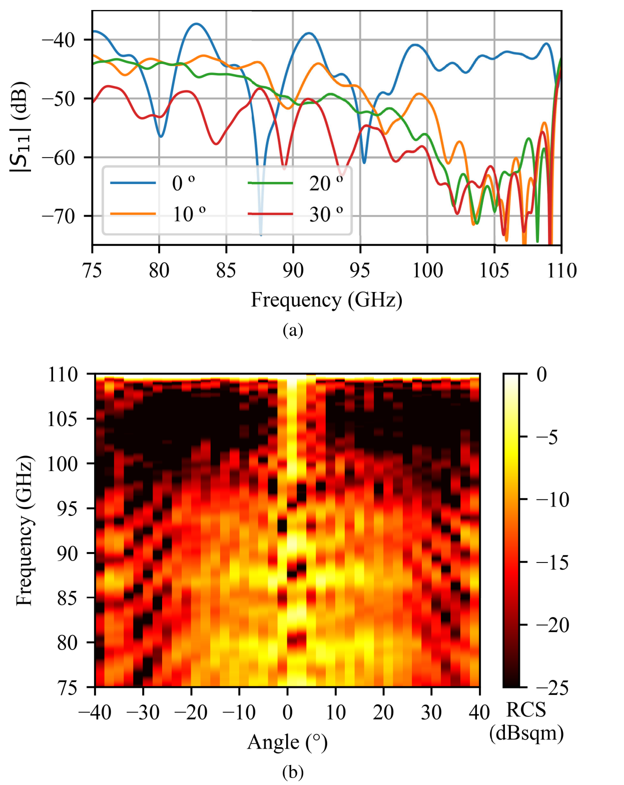

Fig. 5. (a) Measured reflection coefficient, S_{11}, for different angles. (b) RCS over azimuth angles ±40° for FSS-coded trihedral CR.

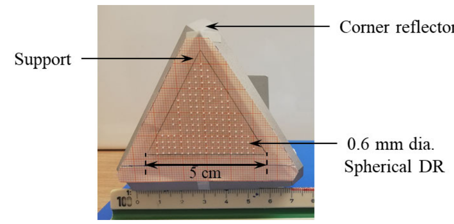

Fig. 6. Frequency-coded CR by spherical DR array.

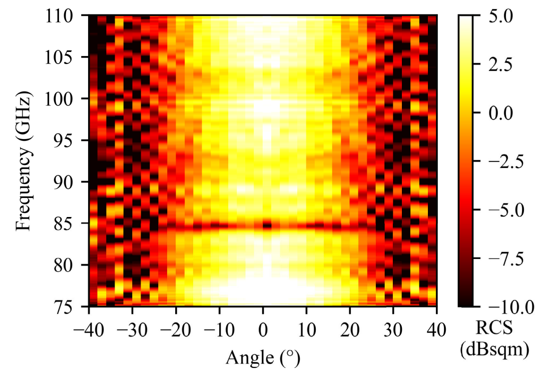

Fig. 7. RCS over azimuth angles ±40° of trihedral CR with DR array coding.

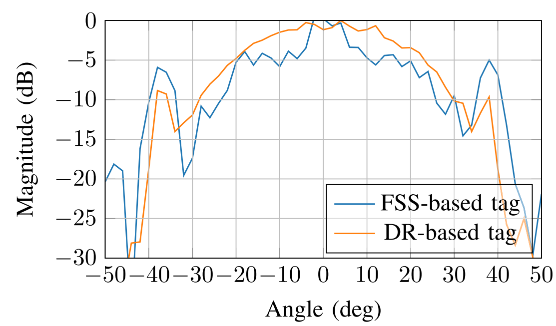

Fig. 8. Normalized RCS for passive chipless tags.

the backscattered signal inside the CR, creating a standing wave. Finally, the mixing of the FSS's specular reflection and the landmark's backscattered response spans between ±6°.

B. DR Array

In this approach, a DR array, instead of the FSS structure, is attached to the trihedral CR surface as seen in Fig. 6. A planar array of spherical DRs is used with a triangular shape of 5 cm edge length (158 elements). The DRs are spaced 2.5 mm in the vertical and horizontal directions. Resonators with a diameter of 0.6 mm and dielectric permittivity of 32 (ZrO^2 ceramic material) are employed to realize the resonance at about 86 GHz. The DR array is placed on a trihedral CR that has an edge length of 7 cm, where the array is placed inline to the opening symmetrically. Details on the operation and characterization of this coded reflector can be found in [25].

The measured RCS spectra are plotted in Fig. 7 in the range −40° to 40°. It is seen that the notch is kept over all angles in the range −20° to 20° where the notch is represented by a line of low RCS. Outside the notch, a large structural RCS of the trihedral CR is dominated.

C. Landmark Comparison

The two presented landmarks have different advantages and challenges when considering their use as part of an indoor self-localization system. These differences can be summarized in terms of 1) readout range; 2) fabrication technology; and 3) coding capacity.

In terms of range, a normalization factor is included in the RCS computation, due to the different size of the CRs used (3 and 5 cm for the FSS-based and DRA-based landmarks, respectively). This is chosen to be the corresponding σ_{CR} for each CR. Thus, (5) is reduced to

$$\sigma_{\text{landmark, norm}} = \frac{\left|S_{11\_\text{landmark}}\right|^2}{\left|S_{11\_\text{CR}}\right|^2}. \quad (6)$$

In Fig. 8, the normalized RCS results are displayed, where it is appreciated that both the DR-based and FSS-based tags present very similar values, which implies that they will perform similarly in terms of maximum range when miniaturizing the former or scaling up the latter.

The manufacturing technology employed to fabricate the FSS and DR array is relevant from the perspective of implementing several tags within the same indoor environment, as well as their scalability to other frequencies. On the one hand, the FSS is manufactured via lithography, etching the FSS elements in a subtrate. On the other hand, each of the DR is positioned and manually paster to a paper sheet with their positions pre-marked. Therefore, the FSS presents an advantage in terms of easeness of manufacturing and scalability to higher frequencies: since the distance between elements must be kept as precise as possible, manual positioning for the DR array is complex and time-consuming.

As it is appreciable in Figs. 4 and 7, the notch bandwidth is starkly different for the two landmarks, with the DR-based

TABLE II
COMPARISON SUMMARY BETWEEN THE LANDMARKS EMPLOYED IN THIS WORK

	Readout range	Manufacturing technology		Coding capability
		Complexity	Scalability potential	
FSS	✓	Low	High	Low
DR array	✓	High	Low	Slightly higher

one significantly narrower. Therefore, more notches (and in consequence, more bits) are possible to be designed within an arbitrary bandwidth than the FSS-based landmark. This in turn allows for the possibility to deploy more landmarks with different frequency-coded responses within the indoor environment. For example, the number of notches that can be encoded within the W-band for the FSS-based approach is 8 notches, or 3 bits [24], while for the DR-based landmark this number slightly increases to ten notches. In Table II, a summary is displayed, presenting the aforementioned landmark's advantages and limitations.

IV. SINGLE TAG ENVIRONMENT

This section presents the results of indoor mapping, where the environment is equipped with a single passive tag to provide localization of the mobile sensor. The objective is to validate the mapping and localization with the proposed method in consideration of an ideal sensing geometry. The ideality is defined here as there are only two scanning angles, one along the in-room objects and the other along the tag. Here, the focus is on the evaluation of the integration of SAR and localization system.

First, the section described the measurement setup and then presents the results in consideration of a DR-based and FSS-based tag.

A. Experimental Setup

For measurements, a VNA-based setup is implemented in a mono-static configuration. The VNA-based testbed acts as an equivalent reader to more cost-effective and compact frequency-modulated continuous-wave (FMCW) radars [1]. Besides, the FMCW radars for the wide bandwidth of 35 GHz at mmWave region are commercially limited to the research sector. Here, the proposed VNA-based testbed provides a high dynamic range and is suitable for experimental evaluation and the validation of the proposed technique. The validation could be adapted to the specific readers such as the FMCW radar.

In the proposed demonstration, a Rohde&Schwarz ZVA67 VNA is employed, which operates in the frequency range from 10 MHz to 67 GHz. The low-frequency EM waves from the VNA are up-converted by the Rohde&Schwarz ZC110 frequency extender in the desired W-band (75–110 GHz). Further, a rectangular horn antenna of gain ∼25 dB is connected to the extender waveguide flange. In this section, two cases are considered, where in case 1, only DR-tag is mounted in the considered infrastructure for localization and identification. In case 2, only FSS-tag is employed. The sketch of the considered room geometry is shown in Fig. 9(a). As the 2-D mapping is addressed, so the considered geometry represents a room of (length × width) 2 × 2 m. The sensing object is mounted at a reference range of 1.4 m and a SAR trajectory

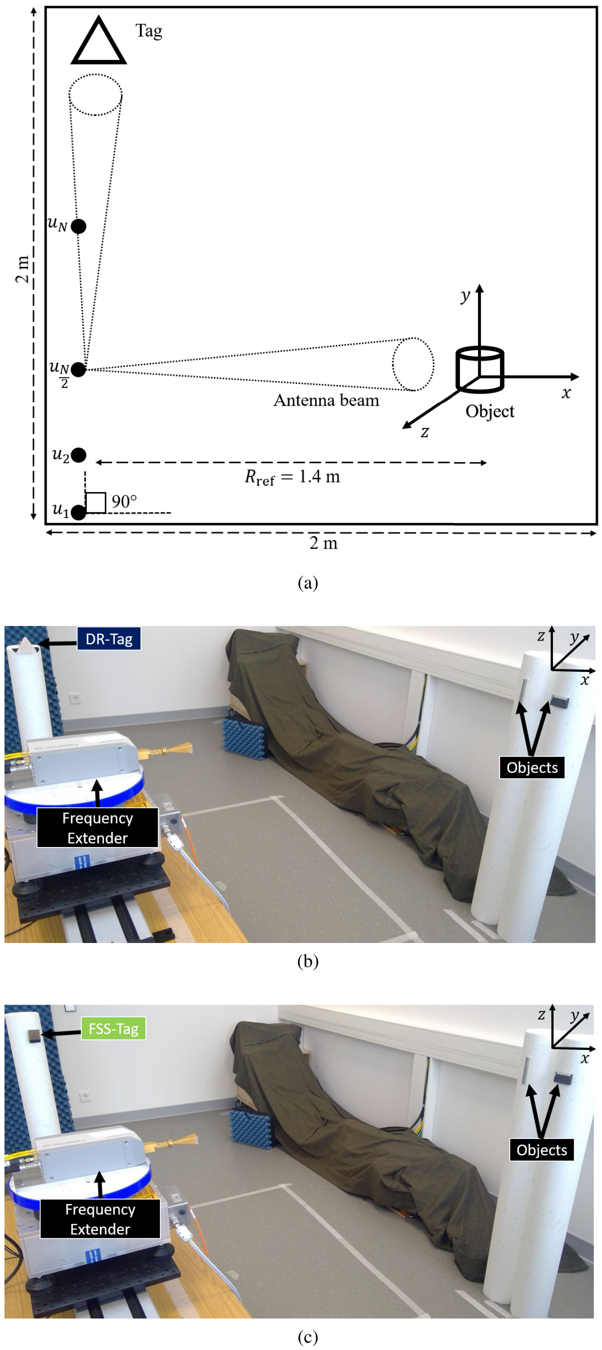

Fig. 9. Measurement setup (a) geometry and pictures with (b) DR-tag and (c) FSS-tag.

is implemented from the azimuth position u_1 to u_N. Here, u_1 corresponds to the origin, position defined as $(x, y, z) =$ (0, 0, 0) m. The localization of the mobile sensor is addressed in reference to this position. The pictures of the measurement setup with DR-tag (case 1) and FSS-tag (case 2) are shown in Fig. 9(b) and (c), respectively. In reference to origin, DR-tag and FSS-tag positions are (0, 1.654, 0) and (0, 1.662, 0) m, respectively. In the presented setup, two imaging objects are considered, where the one is of metallic material in a cylindrical shape with a diameter of 14 mm. Another object is a box of plastic material. It has transparent plastic glass at the front and non-transparent plastic at the back. In this article, the metallic and plastic objects are referred to as objects 1 and 2,

TABLE III
MEASUREMENT PARAMETERS FOR INDOOR MAPPING

Symbol	Parameter	Value
f_c	center frequency	92.5 GHz
B_w	bandwidth	35 GHz
L_a	antenna length	21 mm
$L_{s,c}$	aperture length	40.8 cm
r_x	range resolution	4.3 mm
r_y	azimuth resolution	10.5 mm
R_{ref}	reference range	1.4 m
Δu	step-size	6 mm
N_f	number of frequency points	601
P_b	base transmit power	−10 dBm

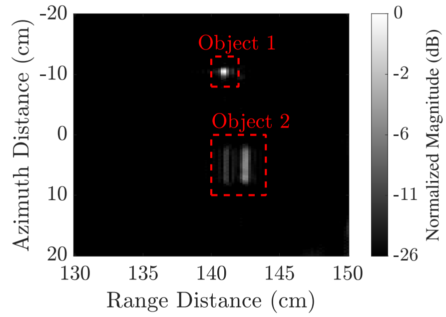

Fig. 10. SAR image as reference image with $\Delta y_{err}(i) \approx 0$.

respectively. Both objects are mounted on a cylindrical foam as shown in Fig. 9.

For SAR trajectory implementation, the frequency extender is mounted on a horizontal stage, which moves along the y-axis with a step size of $\Delta u = 6$ mm. A trajectory length can be considered in accordance to comprehensively mapping the entire indoor environment. Nonetheless, it has been assured that for each mapped object a surrounding trajectory of L_s is based on the employed antenna −3 dB beamwidth [1]. Moreover, with the consideration of SAR integration angle that equals to the beamwidth, the considered step size falls within the conditions defined in [33] and [34]. The measurement parameters are summarized in Table III. Further, to achieve indoor mapping, two simultaneous beams are required as described in Section II-C, which can be acquired using beamforming techniques in MIMO configuration. The presented testbed is limited with a single beam footprint. Therefore, a beam-scanning approach is implemented with the rotation of the transceiver or frequency extender, which is mounted on a turntable. This approach is analogous to a virtual MIMO system. It can be further elaborated using the information or details provided in Fig. 9(a). In reference to the presented Cartesian coordinate system, at each aperture position, imaging objects are excited with EM waves propagating along the x-axis. The backscattered waves are recorded and the frequency extender is rotated by 90° to excite the tag. In this case, the EM waves propagation direction are along the y-axis. This configuration is analogous to a multiple beam scenario. Due to the consideration of an ideal sensing geometry, only two scanning angles 0° and 90° are considered as shown in Fig. 9(a).

For measurements, S_{11} reflection coefficients are captured with a number of frequency points $N_f = 601$. Also, a time-gating correspondence to interested region is applied for removal of standing waves and unwanted reflections. For compensation of the power losses from RF cables, and shifting the reference plane at the extender waveguide flange, one-port short calibration is performed [1]. It is also worth to be noted that an experimental setup is presented for evaluation of the proposed method. Here, the VNA is coupled with extenders via high-frequency cables and adapters, which are not flexible and also very sensitive to bending and movement. Besides, the frequency extender is heavy and to maintain the center of rotation, it needs to be moved slowly. Hence, from the system stability perspective, a quick motion cannot be implemented with the presented setup. For the deployment of the proposed method in a practical environment, it is assumed that lightweight MIMO radars can be used and simultaneously excite the objects and tag with a beamforming approach. So, there might not be a need for the mechanical movement of the sensors. Here, a simultaneous beam setup is implied with the rotation of the sensor, which is analogous to a virtual MIMO concept.

B. Results

Based on the SAR technique, an image of the considered objects is reconstructed and also their respective positions are extracted. For image reconstruction, the trajectory estimation is provided by the localization system. The estimation of the ith aperture position is defined by

$$y_{est}(i) = y_{real}(i) + \Delta y_{err}(i) \quad (7)$$

where $y_{real}(i)$ is the real/actual trajectory position and $\Delta y_{err}(i)$ is the deviation in the estimated position.

For evaluation of the mapped environment with the proposed approach, Fig. 10 shows the generated SAR image of the target in consideration of real trajectory, where $\Delta y_{err}(i) \approx 0$ and hence $y_{est}(i) \approx y_{real}(i)$. In the resulting high-resolution SAR image, both objects are clearly visible and also marked with red rectangles as shown Fig. 10. For object 2, both the front and the back surfaces are obtained due to the penetration capabilities of EM waves at the mmWave spectrum. However, the EM waves cannot penetrate metal. Therefore, for object 1, only the front surface is obtained. Here, Fig. 10 is termed as reference image and the images generated with the proposed approach are evaluated in comparison to this reference image. Further, for mmWave indoor mapping demonstration assisted with localization system, the measurements are recorded as per the setup explained in Section IV-A. In case 1, where a DR-tag is employed, the gathered frequency-domain response for all the aperture positions is shown in Fig. 11. A notch at 85 GHz is obtained, which validates the identification of the tag. The data is processed with the method explained in Section II-B and the aperture positions y_{est} are estimated. Also, an equalization procedure is performed, where the estimated vector is subtracted with the average of the estimations. Fig. 12(a) shows the Δy_{err} based on estimated and real positions. Here, the average absolute error $\bar{y}_{err} = 0.42$ mm. The estimated trajectory is used for SAR image reconstruction of the raw data gathered at a scanning angle of 0°. The resulting SAR image is shown in Fig. 12(b) and the image is accurately mapped and similar to the reference image shown in Fig. 10.

Similar to case 1, in case 2, for localization, FSS-tag is employed and the trajectory is estimated. Fig. 13(a) shows

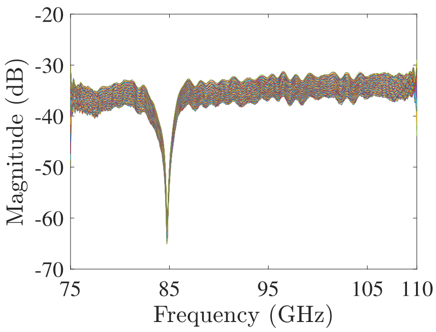

Fig. 11. Frequency-domain response for all the aperture positions with a scanning angle of 90°.

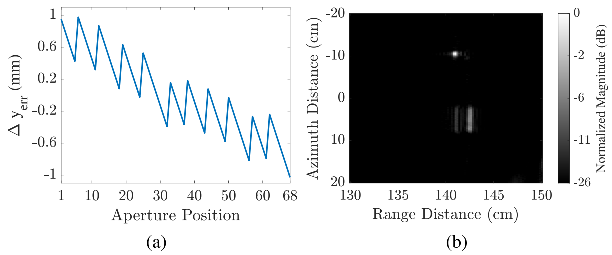

Fig. 12. (a) Δy_{err} based on trajectory estimation in case 1 and (b) reconstructed SAR image with estimated trajectory.

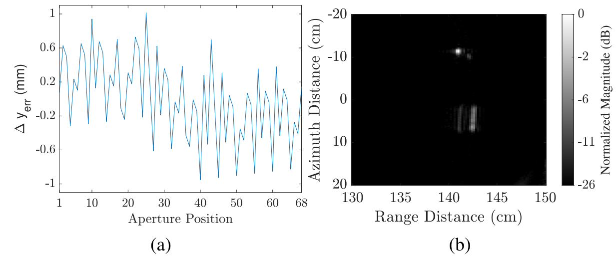

Fig. 13. (a) Δy_{err} based on trajectory estimation in case 2 and (b) reconstructed SAR image with estimated trajectory.

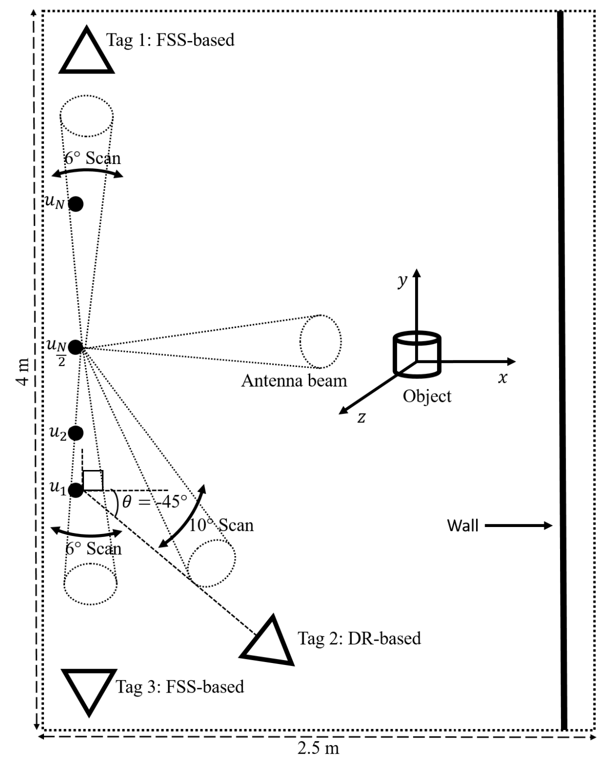

Fig. 14. Measurement setup geometry of mmWave indoor mapping in a multitag environment.

the Δy_{err} calculated with the estimated positions and $\bar{y}_{\text{err}} = 0.39$ mm. Based on the trajectory estimation, the resulting SAR image is shown in Fig. 13(b). For both cases, similar images are acquired. Hence, the proposed approach of indoor mapping is validated.

In terms of computational complexity, the proposed 2-D SAR mapping integrated with the localization system is not highly time-critical application and can be effectively processed in real time. For example, in the case of SAR sensing, the computational complexity is $N \times N_x \times N_y$, where N_x and N_y are the number of image pixels in the range (x-axis) and azimuth (y-axis) directions, respectively. Moreover, the computational time is closely linked to the selection of computing platform such as central processing unit CPU, graphics processing unit (GPU), and field-programmable gate array (FPGA). It is also related on parallel processing model and memory management resources. In the context of UAV-based SAR, where energy resources are a critical consideration, an FPGA-based computational platform looks promising due to its potential for energy-efficient processing. In [35], we have introduced an FPGA-based hardware accelerator and demonstrated SAR image processing execution in a matter of hundreds of milliseconds. Considering a speedup of 86x in comparison to MATLAB execution, a rough approx. of computation time for the presented SAR image would be sub-5 ms. A detailed analysis concerning accelerated implementation on a FPGA platform is available in [35].

V. Multitag Environment

In Section IV, mmWave indoor mapping is demonstrated considering the ideal scenario, where the perfect scanning angles for tag identification are known. This section presents the localization within a multitag environment and finds the suitable angles for tag identification by performing a large degree of beam scanning. Fig. 14 presents the sketch of the indoor mapping scene. Three tags are utilized, where one is the DR-based tag and the other two are FSS-based tags. Here, tags 1 and 2 are the same tags used in Section IV which have the resonance frequency at 105 and 85 GHz, respectively. Tag 3 is FSS-based, similar to tag 1, but with resonance frequency at 90 GHz, achieved by re-scaling the FSS's parameters presented in Table I by a factor of 1.187. There are three objectives of the multitag environment. The first is to enhance the coverage. In a real environment, there will be many cases where no suitable link exists between the sensor and tag. Second, to investigate the compatibility of the proposed method in consideration of a hybrid tag-based environment and to identify tags at different resonance frequencies. Hence, both types of tags, DR- and FSS-based, are used. Third, the focus is on increasing the localization accuracy.

Based on the proposed room geometry in Section IV-A and also shown in Fig. 14, tag 1 (FSS-based), tag 2 (DR-based), and tag 3 (FSS-based) are located at (0, 1.876, 0), (1, −1, 0), and (0, −1.4, 0) m, respectively. From the reference position (0, 0, 0) at u_1, an angle of −45° is formed between the sensor as frequency extender and DR-tag. The angle is shifted based on the aperture position. The tags rely on a frequency-coded

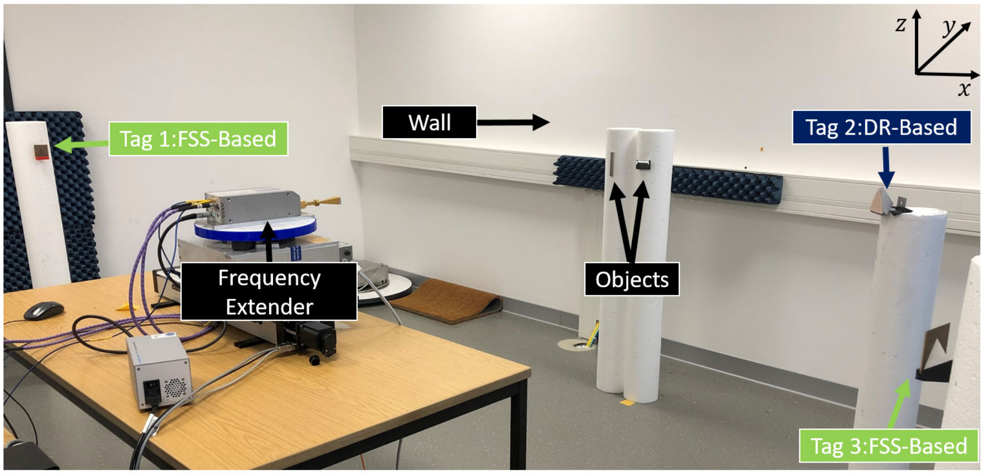

Fig. 15. Measurement setup pictures of mmWave indoor mapping in a multitag environment.

backscattered response from a CR, i.e., deviations from the CR axis decrease the echoes amplitude received at the sensor antenna, as presented in Section III, Fig. 8. However, the sensor is being displaced along different aperture positions, which implies that, when only a fixed scanning angle is taken, the captured response of the tags is non-optimal. Thus, knowledge of the best suitable angles is required throughout the trajectory.

The protocol for the scanning is to make a first initial 360° scan from the reference or initial position to estimate the reachable number of landmarks, their respective slant range and type (FSS- or DR-based). For identification of the type, a cross correlation operation can be performed using a reference signal, and the recorded response can be categorized based on a specific threshold. The proposed system employs only two types of tags and responses differ in terms of notch bandwidth as described in Section III-C. By considering the reference signal as the ideal frequency response of the DR-tag, it is estimated that the cross correlation between the FSS-tag response and this reference signal is less than 50% of the magnitude of the cross correlation with the DR-tag response. Therefore, this can be utilized as the threshold in this context. Further, based on the acquired information, a scanning angle set $\theta_s \in \{\theta_1, \theta_2, \ldots\}$ can be defined in consideration of trajectory, antenna beamwidth, diversity gain, and real-time application. The diversity gain can be achieved by scanning a landmark from multiple angles, which improves landmark identification and hence localization accuracy. Along the SAR trajectory, if the tag is not reachable at a certain aperture position, the scanning protocol can be re-initiated and θ_s should be updated. The employed VNA-based testbed is sensitive to large scanning angles due to phase variations resulting from the bending of cables. Therefore, for the experimental setup, it is assumed that with the initial scan of 360°, three tags are reachable in the environment. Considering the linear SAR 1-D trajectory and diversity gain, for tag 1, a 6° scan ranges from 87° to 90° is selected. For tag 2, the optimal again varies at each aperture position. Therefore, in agreement with the antenna beamwidth of ~10°, a 10° scan in the range of −43° to −52° is implemented. Similar to tag 1, for tag 3, a 6° scan ranging from −87° to −92° is considered as shown in Fig. 14. The proposed VNA-based testbed is well suited for experimental evaluation and validation of methodology. In a practical environment, compact FMCW radar sensors, which offer a very good compromise between accuracy and measurement rate, can be deployed. In the aforementioned W-band, silicon-germanium IC-based radar transceiver is presented in [36]. It covers the frequency range from 68 to 93 GHz and therefore offers a theoretical resolution of approx. 7 mm. The achievable measurement rate, addressing the full system bandwidth, is 1 kHz and could even be further increased at the cost of reduced bandwidth. Using a high-gain dielectric lens antenna [37] of 6° opening angle, a complete 360° scan can therefore be theoretically achieved in 60 ms but is additionally limited by the mechanical scan speed. Due to the compact size of the module, a multiangle monostatic setup is possible that further reduces the scan time. The ability to measure the frequency-dependent reflection coefficient of the DR array was already shown in [38] and allows for the identification of landmarks. Besides, considering the real-time application, SAR imaging can be accelerated with hardware design as presented in [35].

The picture of the implemented multitag testbed is shown in Fig. 15. Regarding the mapping of objects with SAR technique, here a wall is also considered in mapping. In general, based on the SAR trajectory, any object in the environment can be mapped. For the presented experimental setup, only the objects and wall are in the x-y mapping plane. Based on the presented geometry in Fig. 14, measurement data is acquired for localization and mapping, where the collected data at each aperture position is used to identify the tag and also to range. Notch detection algorithm similar to [27] is used to identify the tag from the collected data, where the maximum-likelihood detection is used. Further, when the notch is decided, the best-fit measurements are used for ranging, where the distance is averaged over the chosen measurements.

Fig. 16(a) shows the Δy_{err} in the case of a trajectory estimation in a multitag environment and $\bar{y}_{\text{err}}$ is 0.23 mm. With the increase in the number of tags, higher localization accuracy is expected and hence validated with the presented results. Besides, with the presented setup, the estimation of x-axis coordinates is also explored to address the 2-D localization of the mobile sensor. For the considered geometry of indoor mapping with SAR technique, there is no movement along the

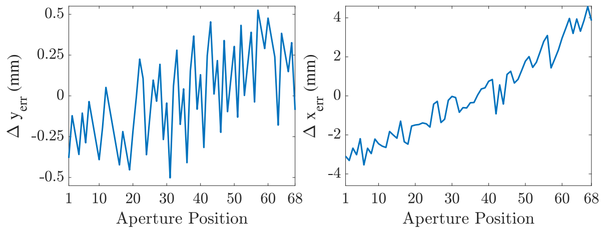

(a) (b)

Fig. 16. (a) Δy_{err} (b) Δx_{err} based on trajectory estimation in multitag environment.

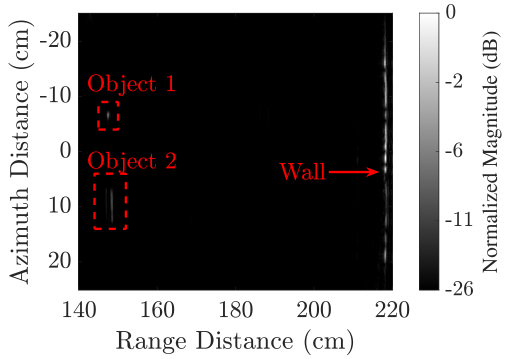

(a)

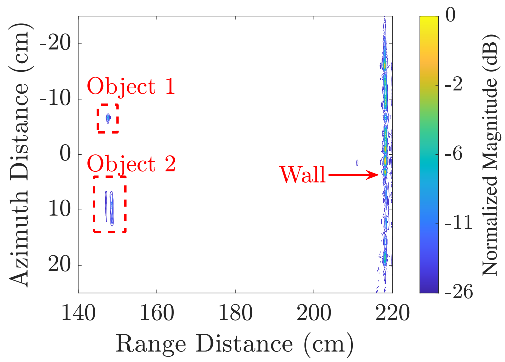

(b)

Fig. 17. (a) Reconstructed SAR image with estimated trajectory (b) SAR image contour.

x-axis and hence it can be considered as a constant x_{real} for the whole trajectory. In accordance with the reference position as center of the coordinate system, the $x_{\text{real}}(u) = 0$ and hence the estimate vector $x_{\text{est}}(u) = \Delta x_{\text{err}}$. Fig. 16(b) shows the x-axis localization estimation error and the absolute average is $\bar{x}_{\text{err}} = 1.8$ mm. It is to be noted here that the x-axis estimation is only performed to address 2-D localization with the presented setup. The implemented setup focuses on precise estimation of the y-axis coordinates, which is required for SAR processing. In analogous to acquired $\bar{y}_{\text{err}} = 0.23$ mm, the estimation accuracy along x-axis can be enhanced by increasing the tags along the x-axis. Also, the accuracy of the estimation along x-axis can be evaluated more precisely with the actual movement of the mobile sensor along x-axis. It is also worth to be noted here that the localization accuracy is also related to the precise knowledge of the reference tags positions in μm scale. However, the current experimental setup is limited with this information as additional components such as laser tracker need to be integrated. In a realistic environment, it is assumed that the information is available under infrastructure planning.

Further, Fig. 17(a) shows the reconstructed SAR image from the estimated trajectory along y-axis. In this case, also, a high-resolution SAR image is obtained, where both the objects and wall are well visible. The RCS from the wall is of higher magnitude than objects and hence its corresponding received power is also larger. Therefore, the wall focusing in the SAR image has a higher magnitude than the objects. In comparison to the reference image shown in Fig. 10, the objects look compressed due to the difference in the range axis plot. In the case of the reference image, the range axis is 20 cm whereas, in Fig. 17(a), it is 80 cm. For better evaluation, a contour plot of the SAR image is shown in Fig. 17(b). Here, objects 1 and 2 along with the wall are well visible. Moreover, the SAR image is extended for the 2-D localization of the mapped objects by extracting range and azimuth profiles. In reference to the presented imaging geometry, object 1 and object 2 are located at (1.476, −0.068) and (1.47, 0.10) m, respectively. Also, a rough estimation can be directly derived from the SAR image.

In summary, multiple tags are identified and the 2-D localization of the mmWave sensor is obtained and an accurate SAR image of the objects present in the environment is generated. Based on the SAR image extension, the 2-D localization of the objects is provided. Hence, the presented results validate the indoor mapping with the proposed method.

VI. Conclusion

The article addressed the indoor mapping at mmWave frequencies. The methodology consists of mapping the environment with SAR technique and estimation of the mobile sensor trajectory with a proposed localization system. The sensor trajectory is calculated by employing two mmWave-based passive chipless tags. They achieve ranging by profiting from the high amplitude echoes generated by CRs while implementing identification of the tags in the backscattered frequency response of the CR utilizing FSSs and DR arrays. Based on the proposed methodology, an experimental setup is implemented and mmWave indoor mapping is demonstrated in consideration of a single-tag and multitag environment. First, in a single-tag environment, integration of the proposed method is evaluated with both tags, and only two scanning angles are implemented. For localization, sub-mm accuracy is obtained. Based on the estimated trajectory, a high-resolution SAR image is obtained, which is equivalent to the best case image where $\Delta y_{\text{err}} \approx 0$. Further, a more realistic approach is considered with a multitag environment. The evaluation is focused on coverage enhancement, hybrid-tag integration, and localization accuracy enhancement. In this approach, the best-suited scanning angles are estimated and measurement data associated with these angles are processed for localization. Similar to the single-tag environment, a high-resolution SAR image is obtained based on the localized trajectory. Besides, the wall in the environment is well mapped. Hence, the presented results validate the proposed method of indoor mmWave sensing.

In future publications, estimation of a 3-D-trajectory by scanning along x-, y- and z-axis and compensation of nonlinear trajectories will be investigated with the proposed scheme.

References

[1] A. Batra et al., "Short-range SAR imaging from GHz to THz waves," *IEEE J. Microw.*, vol. 1, no. 2, pp. 574–585, Apr. 2021.

[2] A. Mostajeran et al., "A high-resolution 220-GHz ultra-wideband fully integrated ISAR imaging system," *IEEE Trans. Microw. Theory Techn.*, vol. 67, no. 1, pp. 429–442, Jan. 2019.

[3] C. Debeunne and D. Vivet, "A review of visual-LiDAR fusion based simultaneous localization and mapping," *Sensors*, vol. 20, no. 7, p. 2068, Apr. 2020.

[4] Y. Xu, Y. Ou, and T. Xu, "SLAM of robot based on the fusion of vision and LiDAR," in *Proc. IEEE Int. Conf. Cyborg Bionic Syst. (CBS)*, Oct. 2018, pp. 121–126.

[5] S. Lee and S. Lee, "Embedded visual SLAM: Applications for low-cost consumer robots," *IEEE Robot. Autom. Mag.*, vol. 20, no. 4, pp. 83–95, Dec. 2013.

[6] D. T. Savaria and R. Balasubramanian, "V-SLAM: Vision-based simultaneous localization and map building for an autonomous mobile robot," in *Proc. IEEE Conf. Multisensor Fusion Integr.*, Sep. 2010, pp. 1–6.

[7] G. Benet, F. Blanes, J. E. Simó, and P. Pérez, "Mapbuilding using infrared sensors in mobile robots," in *New Developments in Robotics Research*. Hauppauge, NY, USA: Nova Science Publishers, 2006.

[8] H. D. Eom and J. W. Jeon, "Environment map building using low-cost IR sensors and a servo motor for mobile robot," in *Proc. 18th IEEE Int. Symp. Consum. Electron. (ISCE)*, Jun. 2014, pp. 1–2.

[9] C. Le, T. Dogaru, L. Nguyen, and M. A. Ressler, "Ultrawideband (UWB) radar imaging of building interior: Measurements and predictions," *IEEE Trans. Geosci. Remote Sens.*, vol. 47, no. 5, pp. 1409–1420, May 2009.

[10] J. Yan, Z. Peng, H. Hong, H. Chu, X. Zhu, and C. Li, "Vital-SAR-imaging with a drone-based hybrid radar system," *IEEE Trans. Microw. Theory Techn.*, vol. 66, no. 12, pp. 5852–5862, Dec. 2018.

[11] I. G. Cumming and F. H. Wong, *Digital Processing of Synthetic Aperture Radar Data*. Norwood, MA, USA: Artech House, 2005.

[12] A. Batra, M. El-Absi, M. Wiemeler, D. Göhringer, and T. Kaiser, "Indoor THz SAR trajectory deviations effects and compensation with passive sub-mm localization system," *IEEE Access*, vol. 8, pp. 177519–177533, 2020.

[13] M. El-Absi, A. A. Abbas, A. Abuelhaija, F. Zheng, K. Solbach, and T. Kaiser, "High-accuracy indoor localization based on chipless RFID systems at THz band," *IEEE Access*, vol. 6, pp. 54355–54368, 2018.

[14] M. Soumekh, *Synthetic Aperture Radar Signal Processing With MATLAB Algorithms*. Hoboken, NJ, USA: Wiley, 1999.

[15] A. Yassin, Y. Nasser, A. Y. Al-Dubai, and M. Awad, "MOSAIC: Simultaneous localization and environment mapping using mmWave without a-priori knowledge," *IEEE Access*, vol. 6, pp. 68932–68947, 2018.

[16] M. Aladsani, A. Alkhateeb, and G. C. Trichopoulos, "Leveraging mmWave imaging and communications for simultaneous localization and mapping," in *Proc. IEEE Int. Conf. Acoust., Speech Signal Process. (ICASSP)*, May 2019, pp. 4539–4543.

[17] J. Palacios, P. Casari, and J. Widmer, "JADE: Zero-knowledge device localization and environment mapping for millimeter wave systems," in *Proc. IEEE Conf. Comput. Commun.*, May 2017, pp. 1–9.

[18] J. Palacios, G. Bielsa, P. Casari, and J. Widmer, "Communication-driven localization and mapping for millimeter wave networks," in *Proc. IEEE Conf. Comput. Commun.*, Apr. 2018, pp. 2402–2410.

[19] A. Shastri et al., "A review of millimeter wave device-based localization and device-free sensing technologies and applications," *IEEE Commun. Surveys Tuts.*, vol. 24, no. 3, pp. 1708–1749, 3rd Quart., 2022.

[20] A. Alhaj Abbas, M. El-Absi, A. Abuelhaija, K. Solbach, and T. Kaiser, "Wide-angle RCS enhanced tag based on dielectric resonator–lens combination," *Frequenz*, vol. 74, nos. 1–2, pp. 1–8, Jan. 2020.

[21] P. Kadera, A. Jiménez-Sáez, T. Burmeister, J. Lacik, M. Schüßler, and R. Jakoby, "Gradient-Index-Based frequency-coded retroreflective lenses for mm-wave indoor localization," *IEEE Access*, vol. 8, pp. 212765–212775, 2020.

[22] A. A. Abbas, Y. Zantah, K. Solbach, and T. Kaiser, "Frequency-coded lens by photonic crystal resonator for mm-wave chipless RFID applications," in *Proc. 4th Int. Workshop Mobile Terahertz Syst. (IWMTS)*, Jul. 2021, pp. 1–5.

[23] A. A. Abbas, M. El-Absi, A. Abuelhaija, K. Solbach, and T. Kaiser, "Corner reflector tag with RCS frequency coding by dielectric resonators," *IET Microw., Antennas Propag.*, vol. 15, no. 6, pp. 560–570, Mar. 2021.

[24] A. Jiménez-Sáez et al., "Frequency selective surface coded retroreflectors for chipless indoor localization tag landmarks," *IEEE Antennas Wireless Propag. Lett.*, vol. 19, no. 5, pp. 726–730, May 2020.

[25] A. Jiménez-Sáez et al., "Frequency-coded mm-wave tags for self-localization system using dielectric resonators," *J. Infr., Millim., Terahertz Waves*, vol. 41, no. 8, pp. 908–925, Aug. 2020.

[26] M. I. Pettersson, "Detection of moving targets in wideband SAR," *IEEE Trans. Aerosp. Electron. Syst.*, vol. 40, no. 3, pp. 780–796, Jul. 2004.

[27] M. El-Absi, A. A. Abbas, A. Abuelhaija, K. Solbach, and T. Kaiser, "Chipless RFID infrastructure based self-localization: Testbed evaluation," *IEEE Trans. Veh. Technol.*, vol. 69, no. 7, pp. 7751–7761, Jul. 2020.

[28] M. El-Absi, A. Al-Haj Abbas, and T. Kaiser, "Chipless RFID tags placement optimization as infrastructure for maximal localization coverage," *IEEE J. Radio Freq. Identificat.*, vol. 6, pp. 368–380, 2022.

[29] F. T. Ulaby, R. K. Moore, and A. K. Fung, *Radar Remote Sensing and Surface Scattering and Emission Theory* (Microwave Remote Sensing: Active and Passive), vol. 2. Reading, MA, USA: Addison-Wesley, 1982.

[30] V. T. Vu, T. K. Sjogren, and M. I. Pettersson, "Phase error calculation for fast time-domain bistatic SAR algorithms," *IEEE Trans. Aerosp. Electron. Syst.*, vol. 49, no. 1, pp. 631–639, Jan. 2013.

[31] Y. Gao, M. T. Ghasr, and R. Zoughi, "Effects of and compensation for translational position error in microwave synthetic aperture radar imaging systems," *IEEE Trans. Instrum. Meas.*, vol. 69, no. 4, pp. 1205–1212, Apr. 2020.

[32] R. Anwar, L. Mao, and H. Ning, "Frequency selective surfaces: A review," *Appl. Sci.*, vol. 8, no. 9, p. 1689, Sep. 2018.

[33] V. T. Vu, D. N. Nehru, M. I. Pettersson, and T. K. Sjögren, "An experimental ground-based SAR system for studying SAR fundamentals," in *Proc. Conf. Asia–Pacific Conf. Synth. Aperture Radar (APSAR)*, Tsukuba, Japan, Sep. 2013, pp. 424–427.

[34] V. T. Vu, Y. Ivanenko, and M. I. Pettersson, "Phase error calculation caused by start-stop approximation in processing FMCW radar signals for SAR imaging," *IEEE Access*, vol. 11, pp. 103669–103678, 2023.

[35] E. Aliagha et al., "Acceleration of 2D SAR imaging on FPGA by reducing off-chip memory accesses," in *Proc. 6th Int. Workshop Mobile Terahertz Syst. (IWMTS)*, Bonn, Germany, Jul. 2023, pp. 1–5.

[36] N. Pohl, T. Jaeschke, and K. Aufinger, "An ultra-wideband 80 GHz FMCW radar system using a SiGe bipolar transceiver chip stabilized by a fractional-N PLL synthesizer," *IEEE Trans. Microw. Theory Techn.*, vol. 60, no. 3, pp. 757–765, Mar. 2012.

[37] N. Pohl and M. Gerding, "A dielectric lens-based antenna concept for high-precision industrial radar measurements at 24 GHz," in *Proc. 9th Eur. Radar Conf.*, Amsterdam, The Netherlands, Oct. 2012, pp. 731–734.

[38] J. Barowski et al., "Design and evaluation of a passive frequency-coded reflector using W-band FMCW radar," in *Proc. German Microw. Conf. (GeMiC)*, Cottbus, Germany, Mar. 2020, pp. 92–95.

Aman Batra (Member, IEEE) received the B.Tech. degree in electronics and communication engineering from Maharshi Dayanand University, Rohtak, India, in 2014, the M.Sc. degree in embedded systems engineering from the University of Duisburg-Essen (UDE), Duisburg, Germany in 2017, and the Dr.-Ing. degree from UDE, in 2021.

He is currently working as a Postdoctoral Researcher at the Institute of Digital Signal Processing, UDE. He is working on terahertz and millimeter wave radar imaging for environmental and biomedical applications. His research interests include digital signal processing, electromagnetic simulations and measurements, hardware-software co-design, computer vision, and high-performance computing.

Dr. Batra is also a part of the organizing committee of the IEEE IWMTS series.

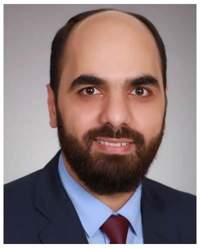

Ali Alhaj Abbas received the B.Sc. degree in electrical/communication engineering from Yarmouk University, Irbid, Jordan, in 2010, the M.Sc. degree from the University of Jordan, Amman, Jordan, in 2016, and the Ph.D. degree from the University of Duisburg-Essen, Duisburg, Germany, in 2020.

From March 2011 to July 2017, he worked as a Teaching Assistant and a Lecturer at Applied Science University, Amman. Currently, he is working as a Researcher at the Collaborative Research Center for the project Mobile Material Characterization and Localization by Electromagnetic Sensing“ (MARIE), Institute of Digital Signal Processing (DSV), University of Duisburg-Essen. His current research interests are in the area of antennas, photonic crystal, UWB antennas, and chipless RFID tags.

Jesús Sánchez-Pastor (Graduate Student Member, IEEE) received the double master’s degree in telecommunications engineering from the Polytechnic University of Valencia, Valencia, Spain, and in information and communication engineering from Technische Universität Darmstadt, Darmstadt, Germany, in 2020, where he is currently pursuing the Ph.D. degree with the Institute of Microwave Engineering and Photonics.

His current research interests include chipless RFID applied to indoor localization and sensing, high-Q photonic crystal cavities, and frequency selective surfaces.

Mohammed El-Absi (Member, IEEE) received the B.E. degree in electrical engineering from the Islamic University of Gaza, Gaza, Palestine, in 2005, the M.S. degree in electrical engineering from the Jordan University of Science and Technology, Irbid, Jordon, in 2008, and the Ph.D. (summa cum laude) degree in electrical engineering from the University of Duisburg-Essen, Duisburg, Germany, in 2015.

He is currently working as a Senior Researcher at the Collaborative Research Center “Mobile Material Characterization and Localization by Electromagnetic Sensing“ (MARIE), Digital Signal Processing Institute, University of Duisburg-Essen. His research interests are in the area of communication and signal processing.

Dr. El-Absi received the Mercator Fellow at the Collaborative Research Center “Mobile Material Characterization and Localization by Electromagnetic Sensing“ (MARIE) from 2017 to 2018 and the German Academic Exchange Service Fellowship in 2006 and 2011.

Alejandro Jiménez-Sáez (Member, IEEE) received the master’s (Hons.) degree in telecommunications engineering from the Polytechnic University of Valencia, Valencia, Spain, and in electrical engineering from the Technical University of Darmstadt (TU Darmstadt), Darmstadt, Germany, in 2017, and the Dr.-Ing. (Hons.) degree in electrical engineering from the TU Darmstadt, in 2021.

His current research interests include chipless RFID, electromagnetic bandgap structures, liquid crystal, and reconfigurable intelligent surfaces.

Dr. Jiménez-Sáez received the Freunde der TU Darmstadt Prize for the best dissertation in electrical engineering and the Athene Young Investigator Award from TU Darmstadt and leads the RF Systems Based on Artificial and Functional Materials Independent Research Group.

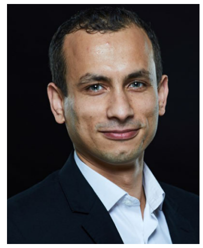

Maher Khaliel received the B.Sc. and M.Sc. degrees in electrical engineering from Benha University, Banha, Egypt, in 2007 and 2012, respectively, and the Ph.D. degree in electrical engineering from the Institute of Digital Signal Processing, Duisburg-Essen University, Duisburg, in 2016.

He was with Benha University as a Teaching Assistance from 2007 to 2012 and a Lecturer from April 2018 to October 2018. He has more than ten years of professional experience at several multi-national companies (Vodafone, CST) in the Middle East area, and he is currently a Senior Developer at ID4us GmbH, Duisburg, Germany, and a Postdoctoral Researcher at the Institute of Digital Signal Processing, Duisburg-Essen University. His Ph.D. research was centered around innovating chipless RFID tags, developing the reader antenna, and integrating innovative approaches to advance the reader functionality.

Dr. Khaliel has published a number of journal/conference papers, nominated for the Best Student Paper Award from European Conference on Antennas and Propagation (EUCAP 2015 and 2017), and was a co-recipient of several awards, including the Best Paper Award of the 15th IEEE International Conference on Communications Systems (ICCS 2016). He joined the Editorial Board of MDPI *Electronic* Journal as a Topic Editor since October 2020, and he also serves as a reviewer for numerous journals like IEEE TRANSACTIONS ON MICROWAVE THEORY AND TECHNIQUES, IEEE TRANSACTIONS ON ANTENNAS AND PROPAGATION, and IEEE JOURNAL OF RADIO FREQUENCY IDENTIFICATION.

Jan Barowski (Senior Member, IEEE) was born in Bochum, Germany, in 1988. He received the B.Sc., M.Sc., and Dr.-Ing. (Hons.) degrees in electrical engineering from Ruhr-University Bochum, Bochum, Germany, in 2010, 2012, and 2017, respectively.

Since 2012, he has been with the Institute of Microwave Systems, headed by Ilona Rolfes, Ruhr-University Bochum, as a Research Assistant, where he is now working as a Postdoctoral Research Scientist at the Institute of Microwave Systems. His research interests include radar signal processing, radar imaging, and material characterization techniques.

Michael Wiemeler received the Dipl.-Ing. degree in electrical engineering from Ruhr-Universität-Bochum, Bochum, Germany, in 1991.

He started in industry and led several development projects for measuring and digital control systems. He was several years with Siemens Mobile Phone, Germany, division in a predevelopment department for Siemens’ UMTS/FDD system prototyping and headed product software integration for mobile phones. Since 2006, he has been with Vodafone D2, Düsseldorf, Germany, in a strategic department defining Vodafone’s technical strategy. He was responsible for spectrum management and technical regulation in national as well as in international bodies (CEPT-ECC). Since 2012, he leads the research group “embedded Signal Processing” Group at DSV, University Duisburg-Essen, Duisburg, Germany.

Diana Göhringer (Member, IEEE) received the master's (Dipl.-Ing.) degree in electrical engineering and information technology and the Ph.D. (summa cum laude) degree in electrical engineering and information technology from the Universität Karlsruhe (TH), Karlsruhe, Germany, in 2006 and 2011, respectively.

She was working as the Head of the Young Investigator Group Computer Aided Design and Exploration of Multi-Core Architectures (CADEMA), Institute for Data Processing and Electronics (IPE), Karlsruhe Institute of Technology (KIT). From 2007 to 2012, she was a Senior Scientist at the Fraunhofer Institute of Optronics, System Technologies and Image Exploitation IOSB, Ettlingen, Germany (formerly called FGAN-FOM). From 2013 to 2017, she was an Assistant Professor and the Head of the MCA (application-specific Multi-Core Architectures) Research Group, Ruhr-University Bochum (RUB), Bochum, Germany. She is a Professor of Adaptive Dynamic Systems, Technische Universität Dresden, Dresden, Germany. She has authored and coauthored over 200 publications in international journals, conferences, and workshops. Her research interests include reconfigurable computing, multiprocessor systems-on-chip (MPSoCs), networks-on-chip, hardware-software-codesign, parallel programming models, and runtime systems.

Dr. Göhringer serves as a technical program committee member in several international conferences and workshops (e.g., DATE, FPL, ICCAD). She is a reviewer and a guest editor of several international journals.

Ilona Rolfes (Senior Member, IEEE) received the Dipl.-Ing. and Dr.-Ing. degrees in electrical engineering from Ruhr University Bochum, Bochum, Germany, in 1997 and 2002, respectively.

From 1997 to 2005, she was with the High Frequency Measurements Research Group, Ruhr University Bochum, as a Research Assistant. From 2005 to 2009, she was a Junior Professor with the Department of Electrical Engineering, Leibniz University Hannover, Hannover, Germany, where she became the Head of the Institute of Radio Frequency and Microwave Engineering, in 2006. Since 2010, she has been leading the Institute of Microwave Systems, Ruhr University Bochum. Her fields of research concern high-frequency measurement methods for vector network analysis, material characterization, noise characterization of microwave devices, sensor principles for radar systems, and wireless solutions for communication systems.

Dr. Rolfes is a member of the Executive Committee of IEEE MTT-S International Microwave Workshop Series on Advanced Materials and Processes. She is a Board Member of the German IEEE MTT-AP Chapter. She is also a Board Member of the German Commission for Electromagnetic Metrology of the International Union of Radio Science (U.R.S.I.). For her research activities she received the European Microwave Price of the European Microwave Conference 2001, the Dr. Heinrich-Kost Award in 2002, within a research consortium the EEEfCOM Innovation Award in 2009, and the IEEE MTT Outstanding Young Engineer Award in 2011. She is the Vice President of the German Association of University Professors and Lecturers (DHV, Deutscher Hochschulverband). She serves as a reviewer for various IEEE transactions and conferences.

Rolf Jakoby (Member, IEEE) was born in Kinheim, Germany, in 1958. He received the Dipl.-Ing. and Dr.-Ing. degrees in electrical engineering from the University of Siegen, Siegen, Germany, in 1985 and 1990, respectively.

In 1991, he joined the Research Center of Deutsche Telekom, Darmstadt, Germany. Since 1997, he has been a Full Professor of Microwave Engineering, Technische Universität Darmstadt, Darmstadt. He has authored more than 599 publications (163 in journals) and holds more than 23 patents. His current research interests include chipless RFID sensor tags, biomedical sensors and applicators as well as tunable passive microwave devices and beamsteering antennas, using electromagnetic bandgap structures, ferroelectric, and liquid crystal technologies.

Dr. Jakoby is a member of VDE/ITG and IEEE/MTT/AP societies. He received the award from CCI Siegen for his excellent Ph.D. in 1992 and the ITG-Prize in 1997 for an excellent publication in IEEE TRANSACTIONS ON ANTENNAS AND PROPAGATION. His group received 26 awards and prizes for best papers and doctoral dissertations. He was the Chairperson of the EuMC in 2007 and GeMiC in 2011, and the Treasurer of the EuMW in 2013 and 2017, respectively. He is an Editor-in-Chief of *Frequenz and DeGruyter*.

Thomas Kaiser (Senior Member, IEEE) received the diploma degree in electrical engineering from Ruhr-University Bochum, Bochum, Germany, in 1991, and the Ph.D. (Hons.) and German Habilitation degrees in electrical engineering from Gerhard Mercator University, Duisburg, Germany, in 1995 and 2000, respectively.

From 1995 to 1996, he spent a research leave with the University of Southern California, Los Angeles, CA, USA, which was grant-aided by the German Academic Exchange Service. From April 2000 to March 2001, he was the Head of the Department of Communication Systems, Gerhard Mercator University, and from April 2001 to March 2002, he was the Head of the Department of Wireless Chips and Systems, Fraunhofer Institute of Microelectronic Circuits and Systems, Duisburg. From April 2002 to July 2006, he was the Co-Leader of the Smart Antenna Research Team, University of Duisburg-Essen, Duisburg. In summer of 2005, he joined the Smart Antenna Research Group, Stanford University, Stanford, CA, USA, and in winter of 2007, he joined the Department of Electrical Engineering, Princeton University, Princeton, NJ, USA, both as a Visiting Professor. From 2006 to 2011, he headed the Institute of Communication Technology, Leibniz University of Hannover, Hannover, Germany. Currently, he heads the Institute of Digital Signal Processing, University of Duisburg-Essen and the Founder and the CEO of ID4us GmbH, an RFID Centric Company, Duisburg. He is the Speaker of the Collaborative Research Center "Mobile Material Characterization and Localization by Electromagnetic Sensing" (MARIE). He has authored and coauthored more than 300 articles in international journals and conference proceedings and two books titled *Ultra Wideband Systems With MIMO* (Wiley, 2010) and *Digital Signal Processing for RFID* (Wiley, 2015).

Dr. Kaiser was the founding Editor-in-Chief of the E-Letter of the IEEE Signal Processing Society and the General Chair of the IEEE International Conference on UltraWideBand in 2008, the International Conference on Cognitive Radio Oriented Wireless Networks and Communications in 2009, the IEEE Workshop on Cellular Cognitive Systems in 2014, and the IEEE Workshop on Mobile THz Systems from 2018 to 2023. He also (co-)founded several Hightech-Startups.